International Immunology, Vol. 28, No. 6, pp. 283–292
doi:10.1093/intimm/dxv072
Advance Access publication 29 December 2015

Lysophosphatidic acid receptors LPA_4 and LPA_6 differentially promote lymphocyte transmigration across high endothelial venules in lymph nodes

Erina Hata[1,2], Naoko Sasaki[1], Akira Takeda[1–3], Kazuo Tohya[4], Eiji Umemoto[1,2,5], Noriyuki Akahoshi[6], Satoshi Ishii[6], Kana Bando[7,8], Takaya Abe[8], Kuniyuki Kano[9], Junken Aoki[9], Haruko Hayasaka[1,2,10] and **Masayuki Miyasaka[1–3,11]**

[1]Laboratory of Immunodynamics, Department of Microbiology and Immunology, Osaka University Graduate School of Medicine, Suita, Osaka 565-0871, Japan
[2]WPI Immunology Frontier Research Center, Osaka University, Suita, Osaka 565-0871, Japan
[3]MediCity Research Laboratory, University of Turku, FIN-20520 Turku, Finland
[4]Department of Anatomy, Kansai University of Health Sciences, Kumatori, Osaka 590-0482, Japan
[5]Laboratory of Immune Regulation, Department of Microbiology and Immunology, Graduate School of Medicine, Osaka University, Suita, Osaka 565-0871, Japan
[6]Department of Immunology, Graduate School of Medicine, Akita University, Akita 010-8543, Japan
[7]Animal Resource Development Unit, RIKEN Center for Life Science Technologies, Kobe 650-0047, Japan
[8]Genetic Engineering Team, Division of Bio-function Dynamics Imaging, RIKEN Center for Life Science Technologies, Kobe 650-0047, Japan
[9]Laboratory of Molecular and Cellular Biochemistry, Graduate School of Pharmaceutical Sciences, Tohoku University, Sendai 980-8578, Japan
[10]Department of Life Science, Faculty of Science & Engineering, Kinki University, Higashi-Osaka-shi, Osaka 577-8502, Japan
[11]Interdisciplinary Program for Biomedical Sciences, Institute for Academic Initiatives, Osaka University, Suita, Osaka 565-0871, Japan

Correspondence to: M. Miyasaka, Interdisciplinary Program for Biomedical Sciences, Institute for Academic Initiatives, Osaka University, Suita, Osaka 565-0871, Japan; E-mail: mmiyasak@orgctl.med.osaka-u.ac.jp

Received 19 August 2015, *accepted* 26 November 2015

Abstract

Naive lymphocytes continuously migrate from the blood into lymph nodes (LNs) via high endothelial venules (HEVs). To extravasate from the HEVs, lymphocytes undergo multiple adhesion steps, including tethering, rolling, firm adhesion and transmigration. We previously showed that autotaxin (ATX), an enzyme that generates lysophosphatidic acid (LPA), is highly expressed in HEVs, and that the ATX/LPA axis plays an important role in the lymphocyte transmigration across HEVs. However, the detailed mechanism underlying this axis's involvement in lymphocyte transmigration has remained ill-defined. Here, we show that two LPA receptors, LPA_4 and LPA_6, are selectively expressed on HEV endothelial cells (ECs) and that LPA_4 plays a major role in the lymphocyte transmigration across HEVs in mice. In the absence of LPA_4 expression, lymphocytes accumulated heavily within the HEV EC layer, compared to wild-type (WT) mice. This accumulation was also observed in the absence of LPA_6 expression, but it was less pronounced. Adoptive transfer experiments using WT lymphocytes revealed that the LPA_4 deficiency in ECs specifically compromised the lymphocyte transmigration process, whereas the effect of LPA_6 deficiency was not significant. These results indicate that the signals evoked in HEV ECs via the LPA_4 and LPA_6 differentially regulate lymphocyte extravasation from HEVs in the peripheral LNs.

Keywords: endothelial cell, high endothelial venule, lymph node, lymphocyte transmigration, lysophosphatidic acid

Introduction

Throughout life, naive lymphocytes patrol the body to detect and eliminate invading pathogens as well as aberrant cells that may arise in the host. During this process, which is called lymphocyte recirculation, the naive lymphocytes selectively migrate into lymph nodes (LNs) and Peyer's patches through a specific type of blood vessel, called the high endothelial venule (HEV). Within the HEVs, naive lymphocytes undergo a multistep adhesion cascade, which is initiated by rolling,

followed by firm arrest and then transmigration. These steps enable the large-scale trafficking of blood-borne naive lymphocytes into the LNs. While the molecular requirements for rolling and adhesion are becoming clearer (1, 2), we still know relatively little about the molecular mechanism of lymphocyte extravasation (3).

Lysophosphatidic acid (LPA) is a pleiotropic lipid mediator that regulates a variety of biological responses, including cell adhesion, migration, proliferation, and survival, gap-junction closure and opening, and the production of growth factors and cytokines (4). LPA can be generated by at least two enzymes: autotaxin (ATX or ENPP2 [ectonucleotide pyrophosphatase/phosphodiesterase family member 2]), which hydrolyzes lysophosphatidylcholine (LPC) to LPA, and phospholipase A_1, which hydrolyzes phosphatidic acid to LPA. There are six known receptors for LPA, LPA_1-LPA_6, which are located on the cell surface (5, 6). LPA_1-LPA_3 are members of the endothelial differentiation gene (EDG) family, which also includes sphingosine-1-phosphate receptor 1 ($S1P_1$), a key regulator of lymphocyte egress from lymphoid tissues (7). LPA_4-LPA_6 are non-EDG family receptors that belong to the purinergic P2Y receptor family (8). These LPA receptors transmit signals through various G proteins, including $G\alpha_i$, $G\alpha_{12/13}$, $G\alpha_q$ and $G\alpha_s$. LPA_1 and LPA_4 are known to be involved in blood vessel formation during development (9). LPA_6 shows high sequence homology with LPA_4; it is expressed in vascular endothelial cells (ECs), where it regulates EC contraction in a $G\alpha_{12/13}$-Rho-dependent manner (5).

Previously, others and we have reported that ATX is highly expressed in the HEV ECs and that it promotes lymphocyte transmigration across the HEVs by locally producing LPA, which in turn acts on HEV ECs (10–12). LPA also acts on lymphocytes to induce chemokinesis, cell polarization and transmigration across HEVs, although the responsible receptor(s) has remained unclear (12, 13).

In this study, we examined the mode of action of the ATX/LPA axis in lymphocyte transmigration across HEVs. We first found that HEV ECs express LPA_4 and LPA_6. Using knockout (KO) mice, we found that LPA_4 deficiency caused severe lymphocyte accumulation within the HEV EC layer, which delayed lymphocyte transmigration across this layer *in vivo*. In contrast, LPA_6 deficiency compromised this cell trafficking process to a much smaller extent. Taken together, these results indicate that LPA_4 and LPA_6 on HEV ECs are differentially involved in the LPA-dependent lymphocyte transmigration across the HEV wall in LNs.

Methods

Mice

C57BL/6 mice were purchased from Japan SLC. GFP transgenic mice (14) were kindly provided by Dr Masaru Okabe (Research Institute for Microbial Diseases, Osaka University). LPA_4 KO mice were generated as described previously (15). The LPA_6/Lpar6 KO mice (Accession No. CDB0977K: http://www.clst.riken.jp/arg/mutant%20mice%20list.html) were generated by three of us (S.I., K.B. and T.A), by crossing $LPA_6^{fl/fl}$ mice and CAG-Cre mice (16), as described in Supplementary Data 1, available at *International Immunology* Online. Homologous recombinants were isolated, using the HK3 ES cell line established from the C57BL/6N strain (17). The LPA_6 KO mice were genotyped by genomic PCR. The primers were 5′-AAAAATCCGAAATGGCAAAGTAAA-3′ and 5′-GTGACCACATCTGAATAGCAAAGG-3′ for the wild-type (WT) allele, 5′-ACTTCCTGACTAGGGGAGGAGTAGA-3′ and 5′-GTGACCACATCTGAATAGCAAAGG-3′ for the floxed allele and 5′-TTCCGTAAACAACATCTCGGTTC-3′ and 5′-GTGACCACATCTGAATAGCAAAGG-3′ for the mutant allele (see Supplementary Data 1, available at *International Immunology* Online, for details) and yielded 303-bp, 445-bp and 462-bp products, respectively. All mice were housed at the Institute of Experimental Animal Sciences at Osaka University Medical School, and all animal experiments followed protocols approved by the Ethics Review Committee for Animal Experimentation of Osaka University Graduate School of Medicine.

Reagents and antibodies

Hybridomas for anti-peripheral node addressin (PNAd) mAb, MECA-79, the anti-mucosal vascular addressin cell adhesion molecule-1 (MAdCAM-1) mAbs, MECA-89 and MECA-367, and the ER-TR7 mAb were injected into nude mice i.p., and the antibodies were later purified from the ascites. Purified MECA-79, MECA-89 and ER-TR7 mAbs were labeled with the Alexa Fluor 594 Protein Labeling Kit (Life Technologies, Carlsbad, CA, USA). The MECA-367 and MECA-89 mAbs were biotinylated using the Sulfo-NHS-LC-biotin Reagent (Thermo Fisher Scientific, Waltham, MA, USA). Anti-ATX serum was generated in rabbits after several immunizations with GST-fused recombinant ATX (57S-116A); its specificity is shown in Supplementary Data 2, available at *International Immunology* Online. Mouse γ-globulins and FITC-anti-α-smooth muscle actin (SMA) mAb were purchased from Sigma-Aldrich (St Louis, MO, USA). Goat IgG, biotinylated anti-CD4 mAb (RM4-5) and allophycocyanin (APC)-anti-CD45 mAb (30-F11) were purchased from Chemicon (Temecula, CA, USA), BD Biosciences (San Jose, CA, USA) and eBioscience (San Diego, CA, USA), respectively. FITC-anti-B220 mAb (RA3-6B2) and purified anti-CD31 mAb (390) were purchased from Biolegend (San Diego, CA, USA). Purified anti-CD31 mAb was labeled with the Alexa Fluor 647 Protein Labeling Kit. Alexa Fluor 647-labeled goat anti-rabbit IgG, Hoechst 33342, lysine fixable FITC-conjugated dextran (MW 70 kDa) and CellTracker™ Orange CMTMR (5-[and-6]-[{(4-chloromethyl)benzoyl}amino]tetramethylrhodamine) were all purchased from Life Technologies.

RT–PCR

HEV ECs were isolated as MECA-367$^+$CD45$^-$ cells from the mesenteric LNs (MLNs) using a FACSVantage cell sorter, and the total RNA was extracted from freshly isolated MECA-367$^+$ HEV ECs using the RNAqueous-4PCR Kit (Ambion, Foster, CA, USA). The cDNA was synthesized using the Ovation System (Nugen Technologies, San Carlos, CA, USA). T cells, B cells and dendritic cells (DCs) were isolated from the spleen as, respectively, CD3$^+$, B220$^+$ and CD11c$^+$ cells. Total RNA was extracted with Trizol (Life Technologies), and cDNA was synthesized with Superscript III (Life Technologies). The cDNA fragments of LPA receptors (*Lpar1-Lpar6*) were amplified by PCR using ExTaq (Takara, Shiga, Japan). The primer

pairs are described in Supplementary Data 3, available at *International Immunology* Online.

In situ hybridization assay

In situ hybridization was performed as previously described (10). The MLNs were embedded in OCT compound (Sakura Finetek, Torrance, CA, USA), and 10-μm-thick serial frozen sections were cut. A 537-bp fragment from nucleotides 182–718 of the LPA_4 cDNA (GenBank accession no. NM_175271) or a 501-bp fragment from nucleotides 23–523 of the LPA_6 cDNA (GenBank accession no. NM_175116) was inserted into the pPCRII vector (Invitrogen). The plasmids were linearized by digestion with *Xho*I or *Spe*I, at sites flanked by the T7 and SP6 promoters, respectively. Digoxigenin (DIG)-labeled anti-sense and sense probes were generated by *in vitro* transcription using the DIG RNA Labeling Mix (Roche Diagnostics, Basel, Switzerland), according to the manufacturer's instructions.

Measurement of body weight and the total cell number in each organ

The total body weight of male 8-week-old LPA_4-deficient mice, LPA_6-deficient mice and their littermates was measured. The total cell numbers in the spleen, MLNs, inguinal LNs (ILNs) and popliteal LNs (PLNs) were determined by flow cytometry (FACSVerse; BD Biosciences).

Conventional immunohistochemistry

ILNs and MLNs obtained from 8-week-old littermate mice were snap frozen in OCT compound and cut into 10-μm-thick frozen sections. The sections were fixed in methanol, blocked in 10% FCS/PBS containing mouse γ-globulins (20 μg/ml) and stained with FITC-anti-α-SMA, Alexa Fluor 594-anti-PNAd, Alexa Fluor 594-anti-MAdCAM-1, biotinylated-anti-MAdCAM-1, biotinylated-anti-CD4, FITC-anti-B220, APC-anti-CD45, Alexa Flour 594-ER-TR7 or Hoechst 33342 (2 μg/ml). Biotinylated antibody was detected by Alexa Fluor 405-streptavidin (2 μg/ml). ATX expression was detected by rabbit anti-ATX serum (1:2000) and Alexa Fluor 647-goat anti-rabbit antibody (2.5 μg/ml) after blocking with goat IgG (20 μg/ml). Immunofluorescence confocal microscopy was performed with an FV1000-D confocal laser scanning microscope (Olympus, Tokyo, Japan) and an LSM 710 confocal laser microscope (Zeiss, Oberkochen, Germany).

Assessment of leakage from HEVs

Mice were given an injection of Alexa Fluor 594-ER-TR7 (5 μg/foot) into the hindfoot. Six hours later, the mice were given an i.v. injection of Alexa Fluor 647-anti-CD31 (10 μg/mouse). Seven minutes later, an i.v. injection with fixable FITC-dextran (MW 70 kDa, 1 mg/mouse) was given. Fifteen minutes after the final injection, the mice were killed under isoflurane anesthesia, dissected and the ipsilateral PLNs were collected in 4% paraformaldehyde (PFA). The LNs were washed with PBS and incubated with 30% sucrose/PBS for 30 min. The immunofluorescent signals were observed with an FV1000-D confocal laser scanning microscope.

Quantification of lymphocyte accumulation within the HEV EC layer

Quantitative analysis of the lymphocyte accumulation within the HEV EC layer was performed using LN sections as follows. The HEV EC layer was identified by staining with fluoresceinated PNAd or MAdCAM-1 mAbs, and the area of the HEV EC layer was determined using ImageJ. Lymphocytes located within the HEV EC layer were identified by CD45 staining, and lymphocyte accumulation within the HEV EC layer was expressed as the number of $CD45^+$ cells per unit HEV EC area (1000 μm^2).

Transmission electron microscopy

The ILNs of 8-week-old WT, LPA_4 KO and LPA_6 KO mice were collected and processed as described previously (18).

Trafficking assay using flow cytometry

Mice were i.v. injected with GFP^+ splenocytes (2×10^7 cells/mouse). Thirty minutes after adoptive transfer, the mice were anesthetized and transcardially perfused with PBS. The spleens, MLNs and peripheral LNs were collected. The proportion of donor GFP^+ cells in these tissues was analyzed by flow cytometry.

Trafficking assay using whole-mount analysis

Mice were i.v. injected with GFP^+ splenocytes (2×10^7 cells/mouse) and an Alexa Fluor 647-conjugated anti-CD31 mAb (10 μg/mouse). Sixty minutes after the injection, the mice were anesthetized and transcardially perfused with PBS and 4% PFA in phosphate buffer. The mice were dissected, and the LNs were harvested. The LNs were incubated with increasing concentrations (10, 20 and 30%) of sucrose. The immunofluorescent signals were observed with an FV1000-D confocal laser scanning microscope (Olympus), and the acquired images were analyzed with the IMARIS 7.4.2. software (Bitplane, Zurich, Switzerland). Briefly, the images were processed using the surface rendering and contour modes.

Statistics

Data are presented as the mean ± SD. Raw data were analyzed using the GraphPad Prism 6 software (GraphPad Software, San Diego, CA, USA). The Mann–Whitney *U*-test was used for comparisons of body weight, the total number of accumulated lymphocytes and lymphocyte extravasation. The Kruskal–Wallis test was used for comparison of the lymphocyte accumulation in three groups before the Mann–Whitney *U*-test. The Student's *t*-test was used for the comparison of lymphocyte trafficking by flow cytometry.

Results

HEV ECs express two LPA receptors, LPA_4 and LPA_6

While we previously showed that the ATX/LPA axis regulates lymphocyte transmigration across the basal lamina of HEVs, primarily by acting on HEV ECs (11), the LPA receptor(s) involved in this event remained unknown. Therefore, we first examined the LPA receptor expression in HEV ECs and leukocytes by RT–PCR. As shown in Fig. 1, HEV ECs, which

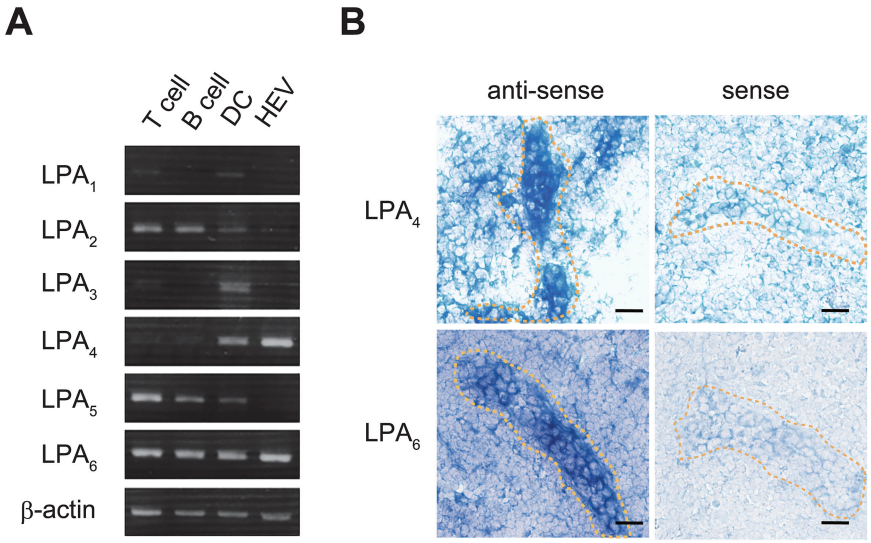

Fig. 1. LPA_4 and LPA_6 are expressed in HEV ECs. (A) HEV ECs were sorted as MECA-367$^+$CD45$^-$ cells from the MLNs. The total RNA was extracted from T cells, B cells, DCs and HEV ECs, and RT–PCR was performed. (B) LPA_4 and LPA_6 expression in MLNs was examined by *in situ* hybridization. Scale bars indicate 20 μm. HEVs are indicated by yellow lines. Data shown are representative of two independent experiments.

were rigorously purified by cell sorting, expressed LPA_4 and LPA_6, whereas lymphocytes expressed LPA_2, LPA_5 and LPA_6, and DCs expressed all of the LPA receptors, at the mRNA level. The LPA_4 and LPA_6 expression on HEV ECs was further confirmed by *in situ* hybridization of LN sections (Fig. 1B). Although we tried to examine the protein expression as well, the commercially available anti-LPA_4 and anti-LPA_6 antibodies we used gave substantial signals not only in WT mice but also in LPA_4 KO and LPA_6 KO mice, indicating that they were not specific enough for our purpose. However, as described later, mice deficient in the *LPA_4* or *LPA_6* gene showed distinct HEV phenotypes compared with WT mice, indicating that the LPA_4 and LPA_6 proteins are indeed functionally expressed in HEV ECs. Although we previously reported that LPA_1 is expressed in HEV ECs (10), that observation was not confirmed in the present study, possibly because of the more rigorous isolation methods used here. These results demonstrated that HEV ECs preferentially express two LPA receptors: LPA_4 and LPA_6.

Neither LPA_4 deficiency nor LPA_6 deficiency grossly affects the LN architecture

To examine the biological significance of the LPA_4 and LPA_6 receptors in the immune system, we next examined the LNs and spleen of WT, LPA_4 KO and LPA_6 KO mice. As shown in Fig. 2(A), neither the LPA_4 nor the LPA_6 deficiency caused a significant difference in the total cell number in the spleen or MLNs. Of the peripheral LNs, while the ILNs and PLNs tended to be larger in the LPA_4 KO mice than in their WT littermates, there was considerable heterogeneity, and no statistically significant difference in the total cell numbers was found. The peripheral LNs of LPA_6 KO mice were comparable in size to those of the WT littermates. In addition, no difference in the total body weight was observed among these groups (Fig. 2A). As shown in Fig. 2(B), immunohistological analysis indicated that neither the LPA_4 nor the LPA_6 deficiency compromised the formation of HEVs, B-cell follicles or T-cell areas in the LNs. FACS analysis of cells obtained from the LNs showed no abnormalities in CD4, CD8 or B220 expression (data not shown).

Injecting a fluoresceinated anti-CD31 mAb intravenously, which illuminated all of the vascular trees in the LNs, revealed no obvious differences in the overall vascular distribution pattern in the LPA_4 KO or LPA_6 KO mice compared to WT mice (Fig. 2C). Intravenously injected FITC-dextran (70 kDa) showed some leakage from HEVs, but most of it was retained within the vasculature at comparable levels in the LPA_4 KO, LPA_6 KO and WT mice (Fig. 2C). The expression of the LPA-producing enzyme, ATX, appeared unaltered in the HEVs and fibroblastic reticular cells of LPA_4 KO and LPA_6 KO mice (Fig. 2B), indicating that the local LPA production was unimpaired. These results indicated that neither the LPA_4 deficiency nor the LPA_6 deficiency grossly affected the tissue architecture or ATX production in LNs.

LPA_4 deficiency and LPA_6 deficiency differentially induce lymphocyte accumulation within the HEV EC layer

Next, to analyze the HEVs of LPA_4- and LPA_6-deficient mice, we examined cross-sections of the PNAd$^+$ HEVs in the ILNs and MLNs of WT, LPA_4 KO and LPA_6 KO mice (Fig. 3A). The HEV ECs, pericytes and lymphocytes were observed by staining for PNAd, α-SMA and CD45, respectively. The PNAd staining appeared sparser and less intense in substantial proportions of the HEVs of the LPA_4 KO and LPA_6 KO mice compared to WT mice (upper panels), which was apparently due to a greater abundance of lymphocytes within the HEV EC layer (lower panels).

To quantify the lymphocyte accumulation, we enumerated the number of lymphocytes within the HEV EC layer per constant HEV area (1000 μm^2) in female mice; the gene dosage effect can be examined in female littermates, because the *LPA_4* gene is located on the X chromosome. As shown in

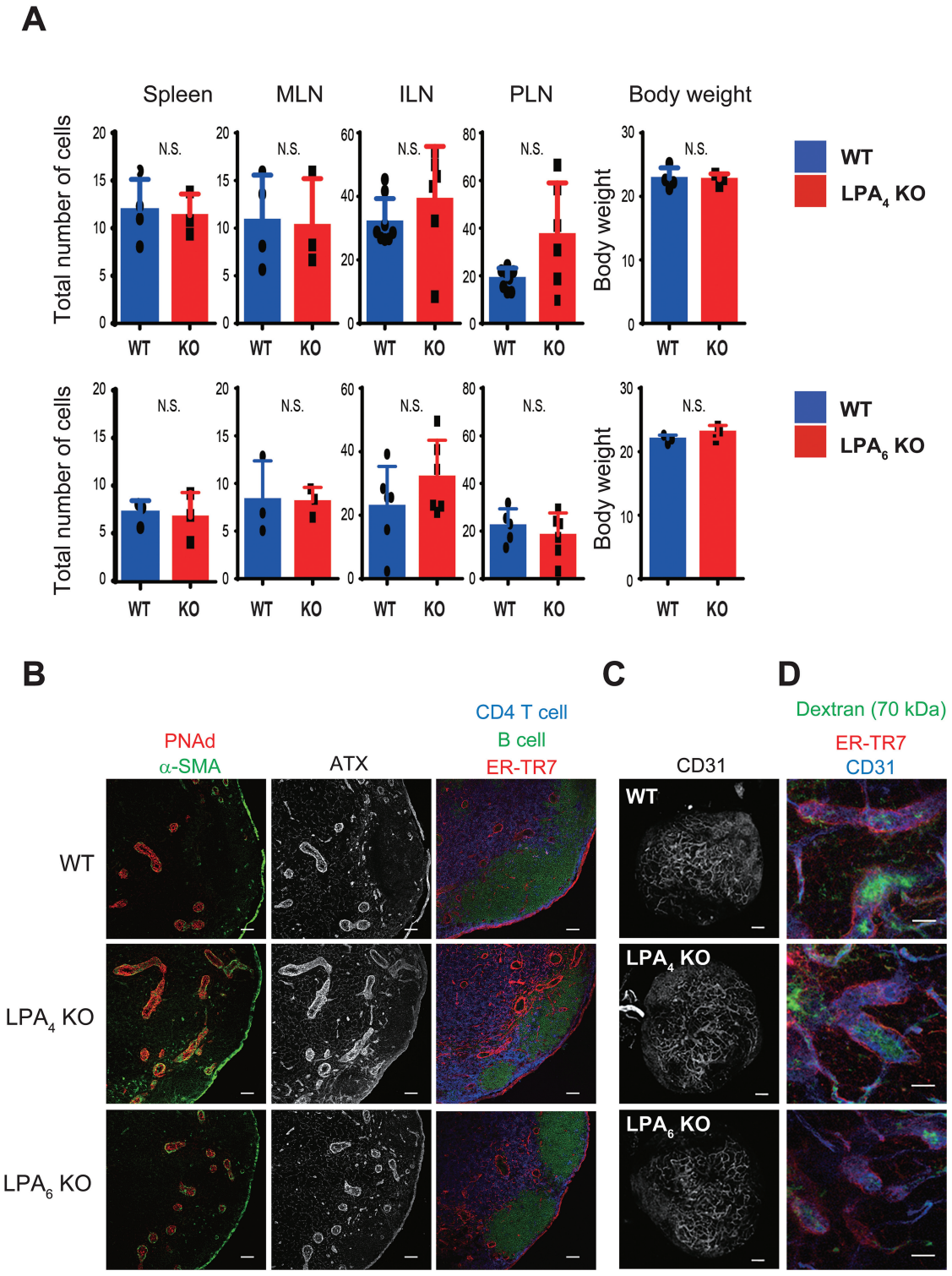

Fig. 2. Neither LPA_4 deficiency nor LPA_6 deficiency grossly affects the LN architecture or ATX production. (A) Total cell numbers of the spleen, MLN, ILN and PLN and total body weight of WT, LPA_4 KO and LPA_6 KO littermates. The cell numbers are shown for the spleen ($\times 10^7$ cells), MLN ($\times 10^6$ cells), ILN ($\times 10^6$ cells) and PLN ($\times 10^5$ cells). Points indicate data from individual mice, and bars show the arithmetic means ± SD for three to four mice from each group. Mann–Whitney *U*-test, N.S.: not significant. (B) Sections of peripheral LNs were stained for CD4 (blue), B220 (green), ER-TR7 (red), α-SMA (green) and PNAd (red). ATX expression was identified by rabbit anti-ATX serum and secondary antibodies (white). Scale bars indicate 50 μm. (C) Blood vessel distribution pattern in the PLN visualized by i.v. injection of the Alexa Fluor 647-anti-CD31 antibody (10 μg/mouse, white). Scale bars indicate 100 μm. (D) HEVs of the PLN visualized by s.c. injection of Alexa Fluor 594-ER-TR7 (5 μg, red) and i.v. injection of anti-CD31 antibody (10 μg/mouse, blue) and FITC-dextran (70 kDa, 1 mg/mouse, green). Scale bars indicate 100 μm. Similar experiments were performed at least three times (LPA_4 KO mice) and once (LPA_6 KO mice) using 2-photon intravital microscopy.

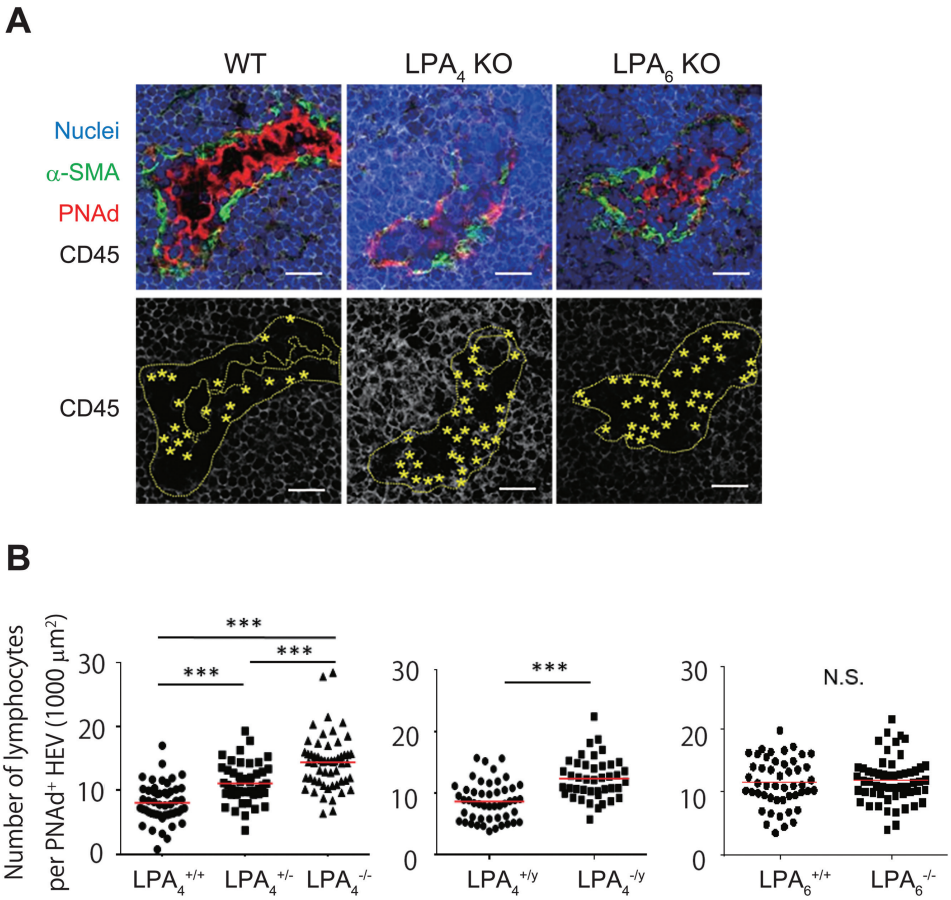

Fig. 3. LPA_4 deficiency and LPA_6 deficiency differentially induce lymphocyte accumulation within the HEV EC layer. (A) Sections of ILNs obtained from WT, LPA_4 KO or LPA_6 KO mice were stained for α-SMA (green), PNAd (red), CD45 (white) and nuclei (blue) and analyzed by confocal microscopy (top panel). Yellow dotted lines and asterisks indicate the HEV EC layer and $CD45^+$ lymphocytes located within the EC layer, respectively (bottom panel). Scale bars indicate 20 μm. (B) Lymphocytes located within the HEV EC layer were enumerated in the ILN obtained from female $LPA_4^{+/+}$, $LPA_4^{+/-}$ and $LPA_4^{-/-}$ mice and from male $LPA_4^{+/y}$, $LPA_4^{-/y}$, $LPA_6^{+/+}$ and $LPA_6^{-/-}$ mice. More than 10 photographs of the ILN section from each mouse were obtained, and three to five mice from each group were analyzed. Kruskal–Wallis test and Mann–Whitney *U*-test, $***P < 0.0001$. N.S.: not significant.

Fig. 3(B), the targeted disruption of LPA_4 increased the lymphocyte accumulation within the HEV EC layer of the ILN in a manner dependent on the extent of gene deletion ($LPA_4^{-/-}$ > $LPA_4^{+/-}$ > $LPA_4^{+/+}$) (left panel). In male mice, the LPA_4 deficiency ($LPA_4^{-/y}$) also significantly increased the lymphocyte accumulation within the HEV EC layer compared with littermate $LPA_4^{+/y}$ mice (middle panel). In contrast, LPA_6 deletion caused only a minimal (statistically non-significant) increase in lymphocyte accumulation within the HEV EC layer (right panel). These results suggested that the LPA_4- and LPA_6-mediated signals are differentially involved in the regulation of lymphocyte transmigration across the HEV wall in peripheral LNs.

Regarding the involvement of LPA_4 signaling, very similar results were observed in the $PNAd^+$ HEV ECs of MLNs (Supplementary Data 4, available at *International Immunology* Online), in which the HEV ECs express either PNAd or MAdCAM-1 as a tissue-specific EC adhesion molecule (19). In the MLNs of both male and female LPA_4 KO mice, elevated lymphocyte accumulation was observed within the EC layer of the $PNAd^+$ HEV ECs, albeit less prominently than in the $PNAd^+$ HEV ECs of the peripheral LNs (Supplementary Data 4, available at *International Immunology* Online). These results together indicated that lymphocyte transmigration across HEVs depends at least partly on LPA_4 signaling in both peripheral LNs and MLNs.

Accumulated lymphocytes in the HEV EC layer are located between the ECs and the underlying basal lamina

We next compared the HEVs of LPA_4 KO, LPA_6 KO and WT mice by transmission electron microscopy. As shown in Fig. 4(A), compared with WT mice, a substantial proportion of the HEVs in both the LPA_4 KO and LPA_6 KO mice contained more lymphocytes within the EC layer, which occasionally caused luminal narrowing. Regarding the precise location of the lymphocytes within the EC layer, it could clearly be seen in the LPA_4-deficient mice that, although some lymphocytes were present between the ECs, most of them were nested between the ECs and the underlying basal lamina (Fig. 4B).

This finding was consistent with an observation reported by Mionnet *et al.* (20), that the HEV ECs create pockets where

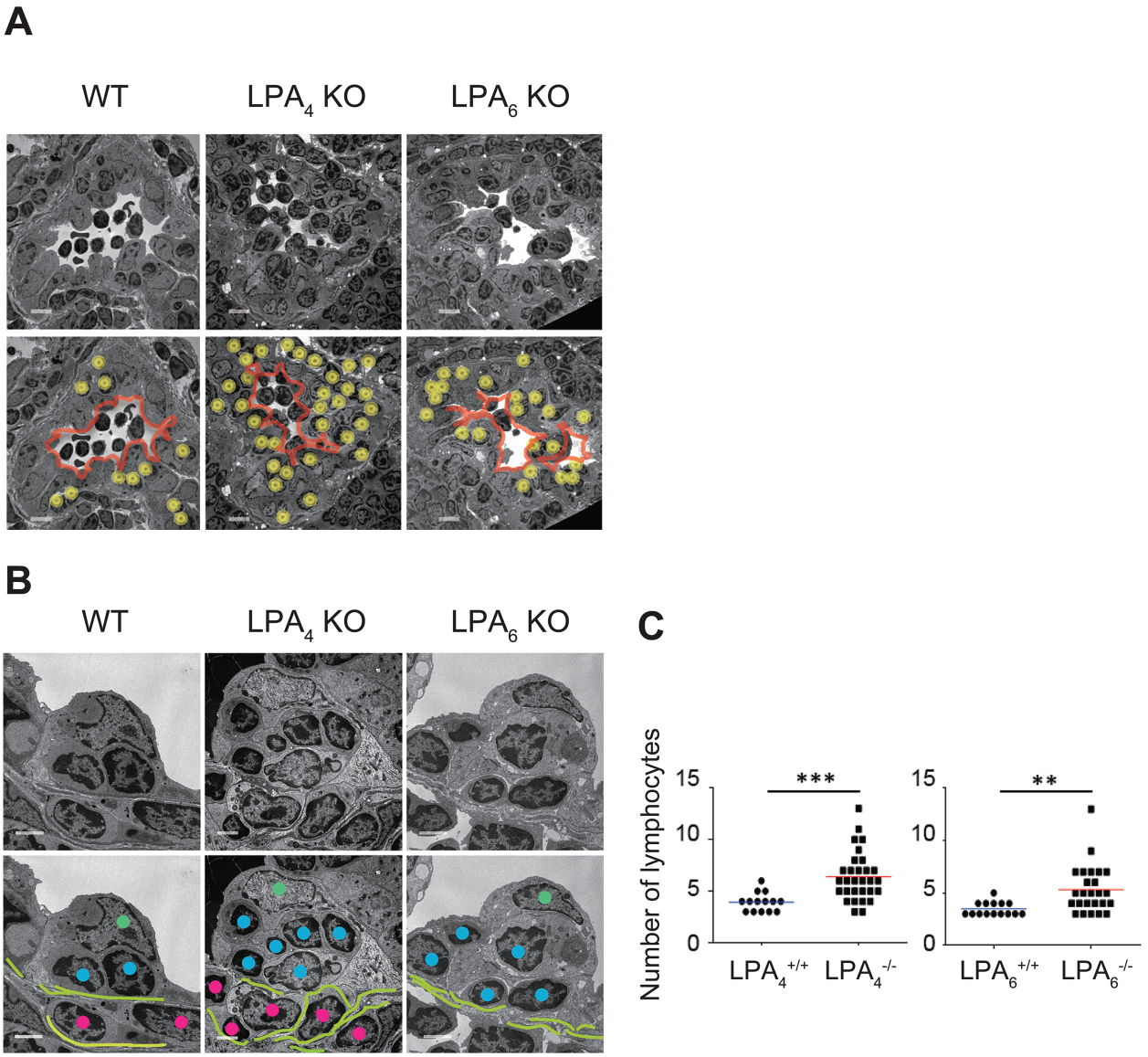

Fig. 4. Lymphocytes are more abundant in the HEV pockets of LPA_4- and LPA_6-deficient mice than in WT mice. (A) Transmission electron micrographs of HEVs in the ILNs of WT, LPA_4 KO and LPA_6 KO mice. Color was added (lower panel of each image) to show that the lymphocytes (yellow) were located in the HEV EC layer including the perivenular channels. The luminal surface of HEV ECs is indicated by red lines. Scale bars, 5 μm. (B) Transmission electron micrographs of HEVs in the ILNs of WT, LPA_4 KO and LPA_6 KO mice. Color was added (lower panels of each image) to show the nuclei of the HEV ECs (green), the discontinuous basal lamina (light green), lymphocytes in the HEV EC layer (blue) and lymphocytes in the vicinity of the basal lamina (red). Scale bars, 2 μm. (C) HEV pockets containing >3 lymphocytes were selected, and the number of lymphocytes per pocket was enumerated in LPA_4 KO, LPA_6 KO and WT littermates. Mann–Whitney *U*-test, $^{**}P < 0.01$, $^{***}P < 0.0001$. More than 10 HEVs in each group were statistically analyzed.

lymphocytes reside for several minutes before they extravasate. These pockets were readily observed in all of the mice we examined, with different degrees of lymphocyte accumulation. Whereas most of the pockets housed up to four to five lymphocytes in WT mice, those in LPA_4 KO and LPA_6 KO mice held statistically greater numbers of lymphocytes (Fig. 4C), with >10 lymphocytes being occasionally present in a single pocket in the LPA_4 KO and LPA_6 KO mice. When this occurred, the ECs overlying such a pocket bulged out into the vascular lumen, resulting in luminal narrowing (Fig. 4A). Given that the pockets in the HEV EC layer are the areas where lymphocytes are retained before they enter the LN parenchyma (20), these data raise the possibility that LPA_4 and LPA_6 are both involved in driving lymphocytes from the pockets into the LN parenchyma.

The absence of LPA_4 signaling delays lymphocyte extravasation across HEVs

To further evaluate the importance of LPA_4- and LPA_6-mediated signaling in the lymphocyte transmigration across HEVs, we adoptively transferred WT donor cells from GFP mice into WT, LPA_4 KO or LPA_6 KO mice and quantified the lymphocyte migration from the blood into the LNs and spleen, by flow cytometry. As shown in Fig. 5(A), LPA_4 deficiency

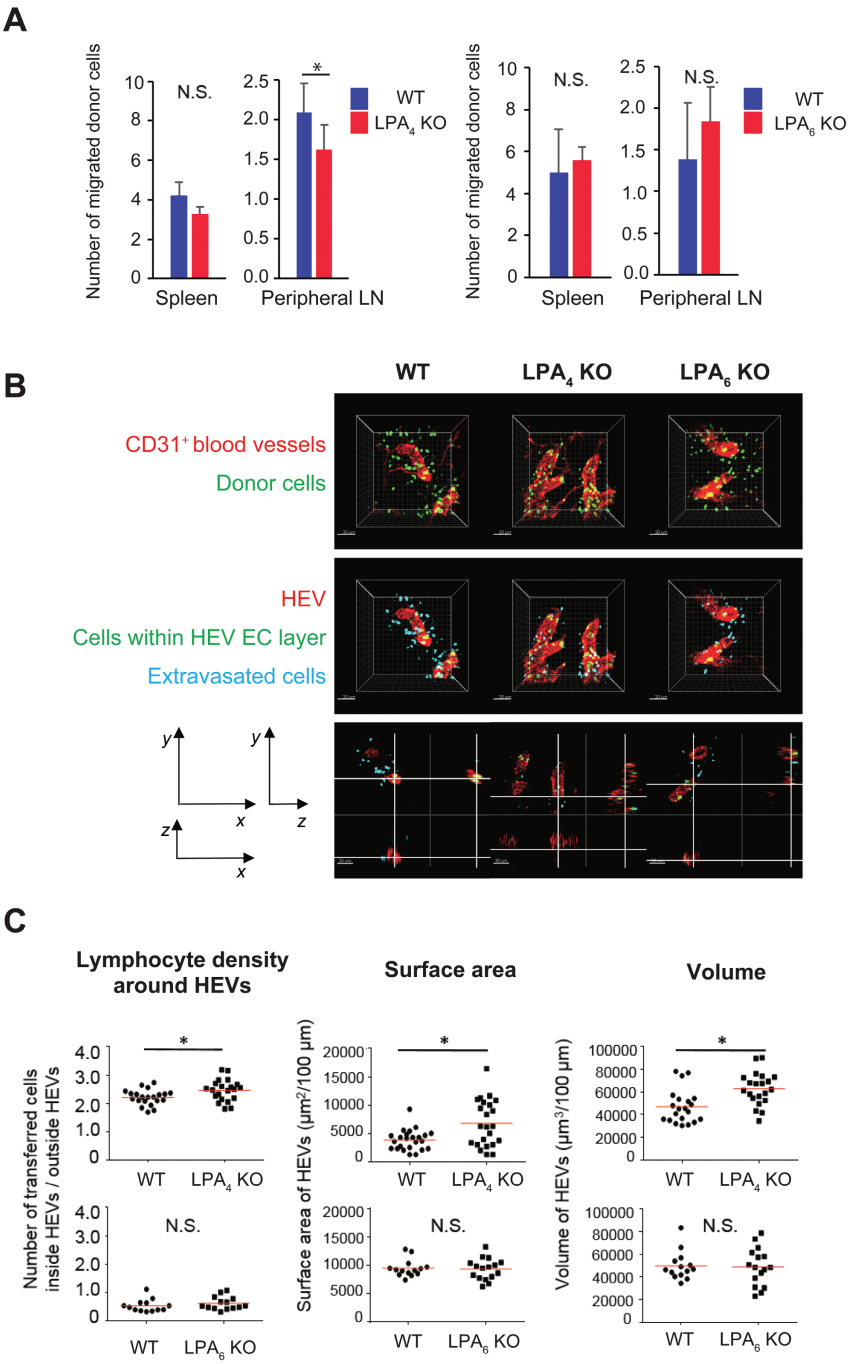

Fig. 5. Lymphocytes accumulate more heavily in the HEV EC layer in LPA_4-deficient mice than in LPA_6-deficient mice. (A) GFP^+ lymphocytes (2×10^7 cells/mouse) were injected into the tail vein of WT, LPA_4 KO and LPA_6 KO mice. Thirty minutes after cell transfer, spleens and peripheral LNs were harvested. The cells that had migrated into these tissues were then quantified by flow cytometry. The number of donor cells found in the spleens ($\times10^5$ cells) and peripheral LNs ($\times10^3$ cells) is shown. Results are shown as the mean ± SD of three mice from each group. Student's *t*-test, N.S.: not significant. The data in the figure are representative of two separate experiments. (B) GFP^+ lymphocytes (2×10^7 cells/mouse) and Alexa Fluor 647-conjugated anti-CD31 mAb (10 μg/mouse) were co-injected into the tail vein of WT, LPA_4 KO and LPA_6 KO mice. Sixty minutes after cell transfer, the mice were perfused with PBS and 4% PFA. The LNs were collected and subjected to confocal microscopic analysis (upper panel; donor cells appear green and $CD31^+$ blood vessels appear red). Subsequently, donor cells within the HEV EC layer and those located within 20 μm of the outside of HEVs were marked in green and blue, respectively, using the IMARIS software (middle panel). $CD31^+$ blood vessels and donor cells in the *xy*, *xz* and *yz* planes (lowest panel). Scale bars indicate 30 μm. The data shown are representative of two separate experiments. (C) Density of transferred cells around HEVs, and the surface area and volume of HEVs in LPA_4 KO, LPA_6 KO and WT mice. Lymphocyte density = the number of donor cells within the HEV EC layer/the number of recently extravasated cells (those located within 20 μm from the outside of an HEV). The HEV surface area and volume per 100 μm of HEV were calculated by the IMARIS software. Mann–Whitney *U*-test, $^*P < 0.05$. N.S.: not significant. The data in the figure are representative of two separate experiments, with two to three mice per experiment.

mildly reduced the lymphocyte entry into the peripheral LNs but not into the spleen, whereas LPA_6 deficiency did not affect the lymphocyte entry into any of the lymphoid tissues examined at appreciable levels. Phenotypic analysis of migrated cells indicated that T-cell migration is more strongly affected than B-cell migration in the absence of LPA_4 signaling (Supplementary Data 5, available at *International Immunology* Online). When LPA_6-deficient cells were transferred to LPA_6-deficient mice, they showed uncompromised migration to the LNs and spleen compared with WT cells (Supplementary Data 6, available at *International Immunology* Online), indicating that LPA_6 in lymphocytes is dispensable for lymphocyte migration *in vivo*.

We next examined whether LPA_4 or LPA_6 deficiency compromised the extravasation of adoptively transferred lymphocytes from HEVs, by the whole-mount analysis of LNs. To this end, we focused on the particular segment of HEVs, termed orders IV-V, where the lymphocyte rolling and subsequent steps preferentially occur (21). We first identified the adoptively transferred lymphocytes and the order IV-V venules in whole-mount LN preparations (Fig. 5B, top panel) and differentially marked the extravasated donor cells located outside but within 20 μm of the HEV basal lamina and those still located within the HEV EC layer, using the IMARIS software (Fig. 5B, middle and lower panels). We then determined the ratio of the cells resident within the HEV EC layer to those recently extravasated from HEVs. This analysis revealed that the LPA_4 deficiency significantly increased the proportion of lymphocytes located within the HEV EC layer (Fig. 5C), in agreement with the results obtained by conventional immunohistological and electron microscopic analyses (Figs 3 and 4), whereas the samples with LPA_6 deficiency did not show a statistical difference from WT.

In addition, reflecting the lymphocyte accumulation within the EC layer, the HEVs of the LPA_4 KO mice had a wider surface area and larger volume compared to those of WT mice, whereas no statistical difference was observed between these data for LPA_6 KO and WT mice (Fig. 5C), although HEVs with a narrowed lumen, apparently due to lymphocyte accumulation within the HEV cell layer, were occasionally found in these mice. In conjunction with the electron microscopy data presented in the previous section, these results indicated that the LPA_4 and LPA_6 receptors play differential roles in the regulation of lymphocyte transmigration across the HEV EC layer, with LPA_4 signaling playing a more influential role than LPA_6 signaling in the HEV ECs.

Discussion

In the present study, we showed that expression of the LPA receptors LPA_4 and LPA_6 on HEV ECs is required for the effective transport of lymphocytes from the HEV EC layer to the LN parenchymal compartment. Without the signal from either of these receptors, lymphocytes were more frequently trapped in the EC layer, where they accumulated in EC pockets and often narrowed the HEV lumen. These results provide new details about the process of lymphocyte transmigration from HEVs by identifying the LPA_4 and LPA_6 receptors as key receptors in this process.

Our whole-mount LN analysis, electron microscopy studies and lymphocyte transfer studies all showed that LPA_4 signaling plays a larger role than LPA_6 signaling in lymphocyte migration through the HEV EC layer. Although we hoped to determine whether this observation could be explained by a difference in their protein expression levels, immunohistochemical analysis failed to produce meaningful results, due to the non-specific reactivity of the commercially available anti-LPA_4 and anti-LPA_6 antibodies we used. Another possible reason for the different effects of LPA_4 versus LPA_6 is a difference in their ligand-binding ability. Yanagida *et al.* (5) showed that LPA_6 has a much lower affinity for LPA compared with other LPA receptors including LPA_4. One can thus envision a situation in which the amount of LPA available in the HEV EC layer determines whether LPA_4 is preferentially stimulated or both receptors are simultaneously stimulated. Not mutually exclusive with these possibilities, it is also possible that LPA_4 and LPA_6 invoke qualitatively different signals in HEV ECs. Previous reports show that LPA_4 activates $G\alpha_{12/13}$- and Rho-mediated signaling in neuronal cells (22, 23). LPA_4 signaling also induces calcium ion mobilization by activating $G\alpha_q$ and $G\alpha_i$, and intracellular cyclic AMP accumulation by activating $G\alpha_s$, which makes this receptor unique among LPA receptors (22). On the other hand, LPA_6 is coupled with $G\alpha_{12/13}$ proteins (5), and its activation leads to increases in intracellular calcium ions and ERK1/2 phosphorylation coupled with $G\alpha_i$ and $G\alpha_{12/13}$ in intestinal epithelial cells (24). While it remains unclear whether LPA_4 and LPA_6 induce different signals in HEV ECs, the development of specific antagonists for LPA_4 and LPA_6 may help resolve this issue.

The LPA_4/LPA_6 receptor requirement for lymphocyte transmigration across HEVs was not absolute, because the HEV ECs deficient in LPA_4 or LPA_6 also allowed lymphocytes to leave the EC compartment and enter the LN parenchyma, albeit to lesser extents compared to those of WT mice. To examine whether LPA_4 and LPA_6 compensate for each other, or if both LPA_4 and LPA_6 are simultaneously required for efficient lymphocyte transmigration across HEVs, we are in the process of generating conventional and conditional LPA_4/LPA_6 double-KO mice.

We previously reported that LPA_1 is expressed in HEV ECs (10), but we did not reproduce this observation in the present study. This discrepancy could be at least partly explained by the fact that in this study, we carefully sorted the HEV ECs to exclude pericytes and smooth muscle cells, which are known to express LPA_1, from the EC preparation.

Upon leaving the HEV luminal surface, naive lymphocytes pass through an endothelial barrier and form pockets within the EC layer (20), where they are transiently retained before being released into the LN parenchyma. In LPA_4- or LPA_6-deficient mice, these pockets contained greater numbers of lymphocytes in substantial proportions of the HEVs compared to WT, although the increase was less obvious in the LPA_6-deficient animals. On the basis of the results of our whole-mount analysis of LNs, we propose that this accumulation was due to a defect in lymphocyte exit from the pockets to the LN parenchyma, and not to an increase in lymphocyte ingress from the HEV luminal surface. One possibility is that LPA_4/LPA_6 signaling promotes the exit process by enhancing the motility of HEV ECs and/or by impeding the strong adhesive interactions between HEV ECs and lymphocytes, allowing lymphocytes to be released from the EC layer more

easily. We had hoped to study the *in vitro* abilities of HEV ECs to support lymphocyte ingress into and egress from the HEV EC layer in the presence or absence of LPA_4 or LPA_6 signaling. However, we have been unable to obtain HEV ECs at sufficient purity for this experiment from mice deficient in LPA_4 or LPA_6, although we could obtain them from WT animals successfully. It could well be that disruption of the LPA_4 or LPA_6 gene has affected the physiology of HEV ECs such that they could not be isolated successfully with the conventional method that we have been using. Future studies focusing on the details of LPA_4/LPA_6 signaling in HEV ECs are still needed.

Despite the slow lymphocyte egress from the EC compartment into the parenchymal compartment, only a minor reduction was observed in lymphocyte entry into the peripheral LNs in the LPA_4-deficient mice, using a conventional lymphocyte trafficking assay. Although the reason for this observation remains unclear, one possibility is the existence of a homeostatic mechanism that regulates overall lymphocyte trafficking efficiency by sensing the trapping of egress-incompetent lymphocytes in the HEV endothelial pockets.

Collectively, these results indicate that LPA_4 and LPA_6 are differentially involved in the LPA-dependent lymphocyte transmigration across the HEV wall in LNs, by signaling through the HEV ECs. As shown previously by our group (11), HEV ECs secrete ATX, which locally converts LPC to LPA; the LPA then acts on HEV ECs in LPA_4- and LPA_6-dependent manners, with the LPA/LPA_4 axis playing a major role. LPA_4 signaling in HEV ECs is thus an interesting target for immunomodulation.

Supplementary data

Supplementary data are available at *International Immunology* Online.

Funding

JSPS Kakenhi (Grant Numbers 21390151, 22021027, 24111005); Grant-in-Aid for JSPS Fellows (Number 25 9108).

Acknowledgements

We thank Norie Yoshizumi for her technical assistance and Prof. Kiyoshi Takeda for allowing E.H. to perform some of her experiments in the Laboratory of Immune Regulation.

Conflict of interest statement: The authors declared no conflict of interests.

References

1 von Andrian, U. H. and Mempel, T. R. 2003. Homing and cellular traffic in lymph nodes. *Nat. Rev. Immunol.* 3:867.
2 Miyasaka, M. and Tanaka, T. 2004. Lymphocyte trafficking across high endothelial venules: dogmas and enigmas. *Nat. Rev. Immunol.* 4:360.
3 Umemoto, E., Hayasaka, H., Bai, Z. *et al.* 2011. Novel regulators of lymphocyte trafficking across high endothelial venules. *Crit. Rev. Immunol.* 31:147.
4 Aikawa, S., Hashimoto, T., Kano, K. *et al.* 2015. Lysophosphatidic acid as a lipid mediator with multiple biological actions. *J. Biochem.* 157:81.
5 Yanagida, K., Masago, K., Nakanishi, H. *et al.* 2009. Identification and characterization of a novel lysophosphatidic acid receptor, p2y5/LPA_6. *J. Biol. Chem.* 284:17731.
6 Choi, J. W., Herr, D. R., Noguchi, K. *et al.* 2010. LPA receptors: subtypes and biological actions. *Annu. Rev. Pharmacol. Toxicol.* 50:157.
7 Cyster, J. G. and Schwab, S. R. 2012. Sphingosine-1-phosphate and lymphocyte egress from lymphoid organs. *Annu. Rev. Immunol.* 30:69.
8 Yanagida, K., Kurikawa, Y., Shimizu, T. *et al.* 2013. Current progress in non-Edg family LPA receptor research. *Biochim. Biophys. Acta* 1831:33.
9 Yukiura, H., Hama, K., Nakanaga, K. *et al.* 2011. Autotaxin regulates vascular development via multiple lysophosphatidic acid (LPA) receptors in zebrafish. *J. Biol. Chem.* 286:43972.
10 Nakasaki, T., Tanaka, T., Okudaira, S. *et al.* 2008. Involvement of the lysophosphatidic acid-generating enzyme autotaxin in lymphocyte-endothelial cell interactions. *Am. J. Pathol.* 173:1566.
11 Bai, Z., Cai, L., Umemoto, E. *et al.* 2013. Constitutive lymphocyte transmigration across the basal lamina of high endothelial venules is regulated by the autotaxin/lysophosphatidic acid axis. *J. Immunol.* 190:2036.
12 Kanda, H., Newton, R., Klein, R. *et al.* 2008. Autotaxin, an ectoenzyme that produces lysophosphatidic acid, promotes the entry of lymphocytes into secondary lymphoid organs. *Nat. Immunol.* 9:415.
13 Zhang, Y., Chen, Y. C., Krummel, M. F. *et al.* 2012. Autotaxin through lysophosphatidic acid stimulates polarization, motility, and transendothelial migration of naive T cells. *J. Immunol.* 189:3914.
14 Okabe, M., Ikawa, M., Kominami, K. *et al.* 1997. 'Green mice' as a source of ubiquitous green cells. *FEBS Lett.* 407:313.
15 Sumida, H. Noguchi, K. Kihara, Y. *et al.* 2010. LPA_4 regulates blood and lymphatic vessel formation during mouse embryogenesis. *Blood* 116:5060.
16 Hayashi, S. and McMahon, A. P. 2002. Efficient recombination in diverse tissues by a tamoxifen-inducible form of Cre: a tool for temporally regulated gene activation/inactivation in the mouse. *Dev. Biol.* 244:305.
17 Kiyonari, H., Kaneko, M., Abe, S. *et al.* 2010. Three inhibitors of FGF receptor, ERK, and GSK3 establishes germline-competent embryonic stem cells of C57BL/6N mouse strain with high efficiency and stability. *Genesis* 48:317.
18 Tohya, K. and Kimura, M. 1998. Ultrastructural evidence of distinctive behavior of L-selectin and LFA-1 ($\alpha L\beta 2$ integrin) on lymphocytes adhering to the endothelial surface of high endothelial venules in peripheral lymph nodes. *Histochem. Cell. Biol.* 110:407.
19 Streeter, P. R., Berg, E. L., Rouse, B. T. *et al.* 1988. A tissue-specific endothelial cell molecule involved in lymphocyte homing. *Nature* 331:41.
20 Mionnet, C., Sanos, S. L., Mondor, I. *et al.* 2011. High endothelial venules as traffic control points maintaining lymphocyte population homeostasis in lymph nodes. *Blood* 118:6115.
21 von Andrian, U. H. 1996. Intravital microscopy of the peripheral lymph node microcirculation in mice. *Microcirculation* 3:287.
22 Lee, C. W., Rivera, R., Dubin, A. E. *et al.* 2007. LPA_4/GPR23 is a lysophosphatidic acid (LPA) receptor utilizing G_s-, G_q/G_i-mediated calcium signaling and $G_{12/13}$-mediated Rho activation. *J. Biol. Chem.* 282:4310.
23 Yanagida, K., Ishii, S., Hamano, F. *et al.* 2007. LPA_4/p2Y_9/GPR23 mediates rho-dependent morphological changes in a rat neuronal cell line. *J. Biol. Chem.* 282:5814.
24 Lee, M., Choi, S., Hallden, G. *et al.* 2009. P2Y5 is a $G\alpha_i$, $G\alpha_{12/13}$ G protein-coupled receptor activated by lysophosphatidic acid that reduces intestinal cell adhesion. *Am. J. Physiol. Gastrointest. Liver Physiol.* 297:G641.